ARTICLE OPEN

Check for updates

Insulator-to-metal transition in ultrathin rutile $VO_2/TiO_2(001)$

D. J. Lahneman[1], Tetiana Slusar[2], D. B. Beringer[3], Haoyue Jiang[1], Chang-Yong Kim[4], Hyun-Tak Kim[2]✉ and M. M. Qazilbash[1]✉

An insulator-to-metal transition (IMT) is an emergent characteristic of quantum materials. When the IMT occurs in materials with interacting electronic and lattice degrees of freedom, it is often difficult to determine if the energy gap in the insulating state is formed by Mott electron–electron correlation or by Peierls charge-density wave (CDW) ordering. To solve this problem, we investigate a representative material, vanadium dioxide (VO_2), which exhibits both strong electron–electron interaction and CDW ordering. For this research, VO_2 films of different thicknesses on rutile (001) TiO_2 substrates have been fabricated. X-ray diffraction (XRD) data show that ultrathin VO_2 films with thickness below 7.5 nm undergo the IMT between rutile insulator below T_c and rutile metal above T_c, while an ultrathin VO_2 film with a thickness of 8 nm experiences the structural phase transition from the monoclinic structure below T_c to the rutile structure above T_c. Infrared and optical measurements on a film of 7.2 nm thickness, below T_c, reveal the energy gap of 0.6 eV in the rutile insulator phase and the absence of the 2.5 eV bonding-antibonding CDW structure. Above T_c, a Drude feature in the optical conductivity reveals the IMT to a metallic phase. These results suggest that for VO_2 films below a critical thickness of about 7.5 nm, the IMT occurs in the rutile structure of VO_2 without the Peierls lattice distortion.

npj Quantum Materials (2022)7:72 ; https://doi.org/10.1038/s41535-022-00479-x

INTRODUCTION

An insulator-to-metal transition (IMT) leads to dramatic changes in physical properties, and it is induced by variation of control parameters such as temperature, chemical doping, and strain[1]. The underlying mechanism of the IMT is ambiguous in materials in which the IMT is accompanied by a structural phase transition (SPT), such as in bulk vanadium dioxide (VO_2)[2–8]. Bulk VO_2 undergoes a thermally induced IMT at the intrinsic critical temperature $T_c \approx 340$ K accompanied by an SPT between a monoclinic (M_1) structure and rutile (tetragonal) structure. The high-temperature metallic phase has rutile structure which is viewed as chains of equidistant vanadium atoms along the rutile c_R-axis. The low-temperature insulating phase has monoclinic (M_1) structure that consists of twisted V-V dimers with alternating spacing of $c_R \pm 2\delta$ (distortion), i.e. the CDW (Peierls) ordering, which generates bonding-antibonding electronic bands. Given the presence of CDW ordering in the M_1 structure, in early works the IMT was considered a Peierls transition[5,6]. However, subsequent experimental and theoretical works demonstrated the significance of electron–electron correlations to the IMT[2–4,9]. Some even posited a new kind of Mott insulator whose ground state is the Peierls ordered phase rather than the antiferromagnetic phase expected in classical Mott insulators[10]. Nevertheless, modern theoretical schemes explain that the IMT and the insulating phase have one aspect in common. Specifically, the calculations in the insulating M_1 phase of VO_2 are based on the Peierls ordered structure and the V-V dimers are considered a necessity for a quantitative description. Indeed, even state-of-the art Dynamical Mean-Field Theory (DMFT) calculations, while emphasizing the significance of electronic correlations, use a cluster-DMFT method based on the primacy of the vanadium pairs[10,11]. This is attributed to the complexity of the electron–electron interactions and the CDW instability in the M_1 structure.

On the other hand, VO_2 films grown on rutile (001) TiO_2 substrates in previous experimental works[12–29] provide an opportunity to consider the IMT in a simpler structure. For thicker VO_2 films grown on rutile (001) TiO_2 substrates, the T_c is close to the intrinsic value of ≈340 K and decreases as the film thickness is reduced. Much of the previous literature has focused on films of thickness equal to or larger than 10 nm and in these films the IMT is accompanied by the SPT[13,16,20]. The electronic IMT in about 4 nm-thick VO_2 films was measured by hard X-ray photoelectron spectroscopy (HAXPES) and X-ray absorption spectroscopy (XAS) but the SPT was not directly measured[28]. A few recent papers have provided evidence in films of reduced thicknesses that the IMT is not accompanied by the SPT[18,22,24]. However, it has been reported that the SPT and the IMT in about 15 nm thick VO_2 film on (001) TiO_2 could occur simultaneously within ±1 K, on the ground that the intensity of the X-ray standing wave sensitively responds to a structural change[26]. In VO_2 films of about 10 nm deposited on (110) and (001) rutile MgF_2 substrates similar to the TiO_2 structure, the SPT between monoclinic and rutile was confirmed by observing Raman scattering[30]. Moreover, in a VO_2 film (thickness of 10 nm) on TiO_2 (001) substrate which can show the SPT between monoclinic and rutile near room temperature, only the IMT was measured, while a VO_2 film (thickness of 5 nm) on TiO_2 (100) substrate did not display the IMT and the SPT near room temperature[31]. Moreover, the orbital assisted metal-insulator transition was suggested in a VO_2 single crystal of much bigger than 7.5 nm thickness, by observing the change of orbital occupation in a manner that charge fluctuations and effective bandwidths are reduced[32]. However, these papers did not directly measure the broadband optical characteristics such as the energy gap which is a defining characteristic of the insulating phase below T_c. Nor did they measure the Drude behavior describing the metallic phase above T_c. Hence, the electronic structure of the ultrathin films of thickness below 10 nm remains unknown.

To address the question about the origin of the energy gap in insulating VO_2, we have grown films of different thicknesses on rutile (001) TiO_2 substrates. We found that films with thicknesses

[1]Department of Physics, College of William & Mary, Williamsburg, VA 23187-8795, USA. [2]Metal-Insulator Transition Lab, Electronics & Telecommunications Research Institute, Daejeon 34129, Republic of Korea. [3]Applied Research Center, College of William & Mary, Williamsburg, VA 23187-8795, USA. [4]Canadian Light Source, 44 Innovation Boulevard, Saskatoon, SK S7N 2V3, Canada. ✉email: htkim@etri.re.kr; mmqazilbash@wm.edu

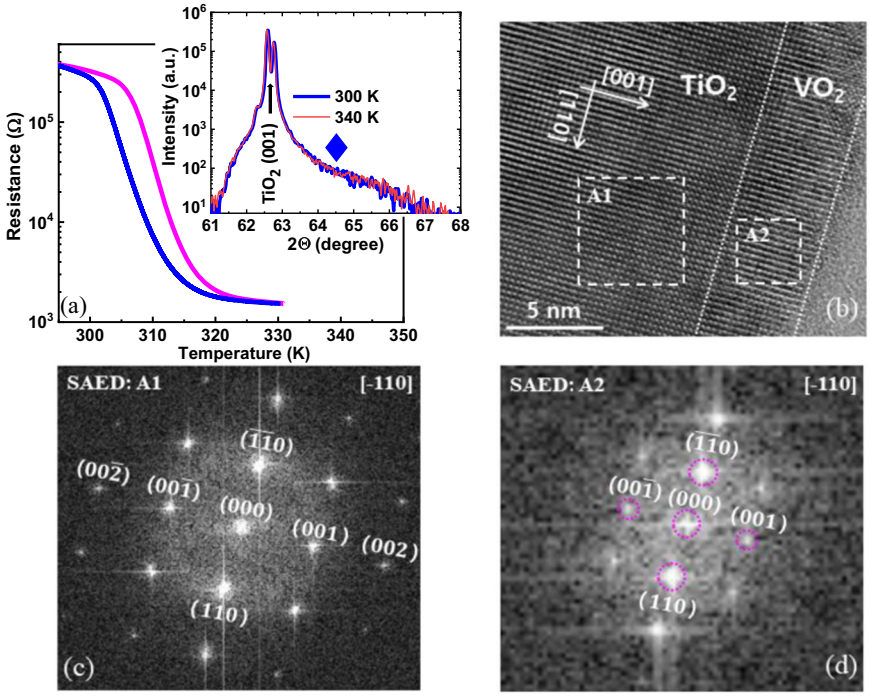

Fig. 1 Transport and structural characterization. Temperature-dependent resistance (R) of ultrathin VO_2 film of a thickness of 7.2 nm on rutile (001) TiO_2. The magenta and blue curves are obtained while heating and cooling the sample respectively. The inset displays the XRD curves. The blue diamond indicates a monoclinic peak position (64.55°, see Supplementary Note 3). Here, the monoclinic peak is not observed in the inset. **b** TEM image of the VO_2/TiO_2 interface demonstrating clear epitaxial growth. Selected area electron diffraction (SAED) images of the white dashed rectangle (A1) in TiO_2 (**c**) and (A2) VO_2 (**d**) from TEM image.

below 7.5 nm are in the rutile structure and the monoclinic distortion induced by CDW (Peierls) ordering is absent[25]. This simplifies the problem because what remains to be confirmed is the lattice structure through X-ray diffraction (XRD) below and above T_c, the energy gap of the insulating phase, and the Drude behavior in the metallic phase following the IMT.

In this paper, we demonstrate a rutile Mott insulator below $T_c \approx 306$ K (Fig. 1a) by observing the absence of a structural change, the energy gap of 0.6 eV, and the absence of the CDW bonding-antibonding optical transition. Furthermore, we observe the IMT via the emergence of the Drude feature above T_c. These observations were enabled by XRD measurements and broadband infrared and optical spectroscopy in a 7.2 nm thick VO_2 film grown on rutile (001) TiO_2 substrate prepared by pulsed laser deposition (see Methods for details). Moreover, we compare the optical conductivity spectra of ultrathin VO_2 films with that of thicker, bulk-like VO_2 films[33]. Synchrotron XRD data reveal that a 6 nm thick VO_2 film has the same rutile structure above and below T_c, and that an 8 nm thick VO_2 film has the M_1 CDW phase below T_c.

RESULTS

Structural and transport properties

Figure 1a shows the resistance–temperature (R–T) curves measured on a 7.2 nm thick VO_2 film on rutile (001) TiO_2 substrate. The inset in Fig. 1a shows X-ray-diffraction (XRD) patterns of the film measured above and below T_c with $\lambda_{Cu} = 1.54056$ Å using commercial, table-top X-ray equipment (see "Methods" for details). Apart from the obvious feature from the rutile (001) TiO_2 substrate, there is a broad feature centered at $2\theta \approx 66°$. The important point is this broad feature shows no temperature dependence at all and is attributed to rutile VO_2 (see Supplementary Note 2 for more detailed data).

Furthermore, an ultrathin VO_2 film of about 5 nm thickness grown on rutile (001) TiO_2 substrate was imaged by transmission electron microscopy (TEM). Figure 1b shows that the crystalline pattern of the film in real space is the same as that of the substrate demonstrating epitaxial film growth. The reciprocal space selected area electron diffraction (SAED) patterns from a region in the TiO_2 substrate and a region in the VO_2 film are compared in Fig. 1c, d; the patterns are the same. These data are consistent with a previous observation that in a thick VO_2 film grown on rutile (001) TiO_2, the first 7.5 nm thickness above the film-substrate interface is in the rutile structure[25]. Moreover, ultrathin VO_2 films grown on rutile (001) TiO_2 exist in the rutile structure[18,22,24,29,34,35]. Thus, the VO_2 film in the insulating phase below T_c has the rutile structure, as shown in the inset of Fig. 1a, and the complexity in the electronic structure due to the CDW is reduced.

In order to improve signal-to-noise in the XRD measurements, we performed XRD measurements on ultrathin VO_2 films at the Canadian Light Source. Figure 2 shows R-T curves and structural characterization of an ultrathin VO_2 film on the rutile (001) TiO_2 substrate. This film is 6 nm thick. The XRD measurements were performed using X-ray energy of 15.120 keV (a wavelength of $\lambda_{Synchrotron} \approx 0.82$ Å) and an exposure time of 600 s. One dimensional detector (Mythen2 1 K from Dectris), able to measure a wide range of two theta angles with one exposure, was used for data collection. Figure 2a shows R–T curves of the 6 nm thick VO_2 film on (001)TiO_2. Thickness of the film has been determined by the film deposition rate. Figure 2b shows the XRD patterns obtained from the 6 nm VO_2 film below (279 K, blue curve) and above (338 K, red curve) the IMT T_c. Here, a large peak 1 ($2\theta \approx 32.2°$) comes from the rutile TiO_2 substrate. A broad peak 2 (33.5°–33.7° depicted by a red arrow in Fig. 2b) corresponds to the rutile (002) VO_2 peak confirmed by the fitting (Fig. 2c, d). Importantly, peak 2 does not shift its position across the IMT demonstrating the absence of the SPT. The possible increase of the VO_2 peak intensity at 338 K may be due to thermal broadening of the large TiO_2 peak[36]. A remarkable fact in Fig. 2b is the absence of the monoclinic (M_1) VO_2 peak near $2\theta = 33°$ at 279 K,

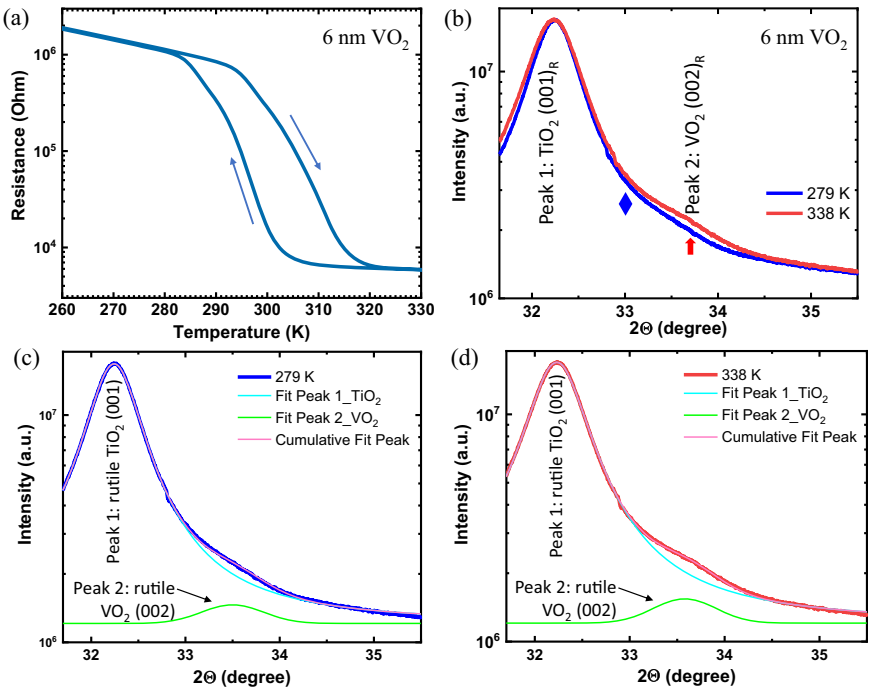

Fig. 2 Transport and structural characterization of a 6 nm thick VO_2 film. a Temperature dependence of resistance of the 6 nm thick VO_2 film on rutile (001) TiO_2. **b** XRD patterns obtained from Synchrotron light source of the sample shown in (**a**) below (blue curve) and above (red curve) the IMT in VO_2. **c**, **d** Fitting details of the data shown in (**b**) are given, which indicate the broad peak is rutile one.

as displayed by a blue diamond in Fig. 2b. The synchrotron XRD data conclusively shows that the 6 nm VO_2 film is in the rutile phase at 279 K (below IMT T_c) and remains in the rutile phase at 338 K (above IMT T_c). Therefore, the IMT in Fig. 2a is not accompanied by the SPT. This is direct evidence of the Mott transition from the rutile insulator phase to the rutile metal phase.

We also performed XRD measurements at the Canadian Light Source on an 8 nm thick VO_2 film on rutile (001) TiO_2 substrate. Thickness of the film has been determined by the film deposition rate. The *R*–*T* and XRD data on the 8 nm thick film are shown in Fig. 3a, b respectively. The XRD data reveals a shift of the VO_2 peak upon increasing the temperature across the IMT. This shows that the top few surface layers of the film undergo a SPT between the monoclinic (M_1) structure and the rutile structure. The SPT is displayed as a shift from $2\theta \approx 33.0°$ the monoclinic (-402) VO_2 peak, observed below IMT (277 K, blue curve), to 33.4°, designating the rutile (002) VO_2 peak above IMT (319 K, red curve). Note that the 8 nm thick film exceeds the critical film thickness of 7.5 nm[25], above which the rutile lattice of the insulating phase relaxes to monoclinic (M_1) lattice.

Infrared and optical properties

Broadband infrared and optical spectroscopy was employed to determine the real and imaginary parts of the frequency-dependent dielectric function in the metallic and insulating phases of the 7.2, 55, and 90 nm thick VO_2 films grown on rutile (001) TiO_2 (see Fig. 4a–c). From the dielectric function, we obtain the optical conductivity. The real part of the optical conductivity (σ_1) is related to the imaginary part of the dielectric function by the equation: $\sigma_1 = \omega\varepsilon_2/(4\pi)$ in CGS units[37]. We plot σ_1 in SI units (Ω^{-1} cm^{-1}) in the insulating and metallic phases of the 7.2 nm thick rutile VO_2 film in Fig. 4a. Peaks in optical conductivity can be attributed to direct optical transitions from a filled band to an empty band. The spectrum below T_c in the insulating phase of the ultrathin VO_2 film shows the energy band feature β centered at 1.3 eV and an energy gap (E_g) of 0.6 eV disappearing during the IMT. The feature β is due to the optical interband transition between the filled, lower a_{1g} band to the empty e_g^{π} band[33]. We also observe a feature ξ with band center 3.2 eV and a feature κ with a band center of 4.4 eV in the optical conductivity of the insulating phase[33].

For the sake of comparison, we have obtained the optical conductivity of two thicker VO_2 films (55 and 90 nm thicknesses) grown on rutile (001) TiO_2 substrates (Fig. 4b, c). The figures show the Y peak corresponding to the peak measured in bulk-like M_1 insulating phase of thick VO_2 film on Al_2O_3 (ref. [33] and Supplementary Fig. 4). When the optical conductivity spectrum of the ultrathin film (Fig. 4a) is compared to the optical conductivity spectra of the thicker VO_2 films (Fig. 4b, c), the similarities include the existence of features X and Z which correspond to features β and ξ, respectively. However, the Y feature with band center of about 2.5 eV, existing in Fig. 4b, c and Supplementary Fig. 4, is not seen in Fig. 4a. The feature Y in the optical conductivity spectra of the M_1 insulating phase is known to be due to optical interband transition between the a_{1g} bonding ($d_{\|}$) and a_{1g} anti-bonding ($d_{\|}^*$) bands generated due to the CDW (Peierls) ordering of V-V dimers[38,39]. Its absence indicates that the ultrathin VO_2 film has the rutile structure without CDW ordering, as also proven by the analysis of the TEM image in Fig. 1b, d and the absence of a structural transition in the XRD data (Fig. 1a, inset). Remarkably, the absence of the Y feature indicates that the formation of both the energy gap of about 0.6 eV and the associated optical interband transition β are independent of the Y feature. This further demonstrates that Peierls ordering is not responsible for the formation of the energy gap of β, leading to the conclusion that the forming mechanism of the energy gap is primarily caused by electron–electron interaction. This is different from the conclusion in ref. [40] that cooperative Mott–Peierls MIT characteristic in bulk VO_2 almost holds down to 2.0 nm thick film grown on Nb-doped (001) TiO_2 although ref. [40] does not include direct measurements of the SPT using XRD and the substrate is different from that used in our work.

The feature κ in the spectrum of rutile insulating VO_2 in Fig. 4a is an optical interband transition, which is not evident in the spectra

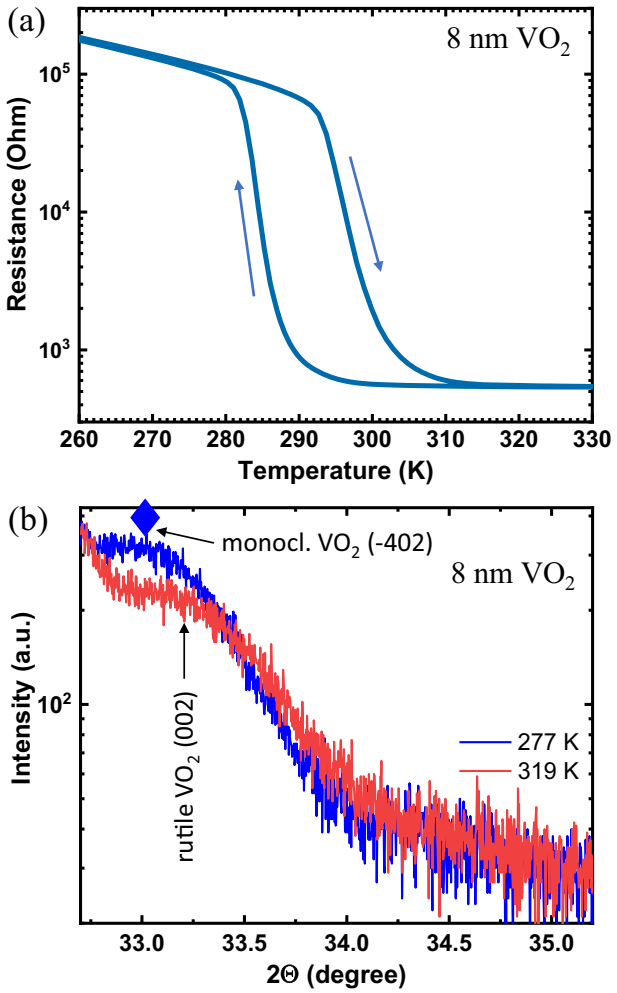

Fig. 3 Transport and structural characterization of an 8 nm thick VO_2 film. a Temperature dependence of resistance of the 8 nm thick VO_2 film on rutile (001) TiO_2. **b** XRD patterns obtained from Synchrotron light source of the 8 nm thick VO_2 on (001) TiO_2 below (blue curve) and above (red curve) IMT.

of insulating M_1 VO_2 (Fig. 4b, c).The feature κ is also seen in the rutile metallic phase (Fig. 4a) and may arise from strong electronic correlations in the strained rutile structure. The feature ξ (and Z) at about 3.2 eV is attributed to the optical transition from the filled O_{2p} band to the empty e_g^π band and from the filled a_{1g} band to the empty e_g^σ band[11,33,41–43].

The optical conductivity spectrum of the metallic state shows that the weak Drude conductivity in the *dc* limit ($\omega \rightarrow 0$) (Fig. 4a) is about a factor of 5 lower than those obtained in the thick bulk-like VO_2 films (Fig. 4b, c). The effective number of delocalized carriers per vanadium atom, N_{eff}^{Drude}, in the metallic state is about four times lower than the value for bulk-like rutile VO_2 metal (see "Methods"). This is primarily because the spectral weight of the free-carrier Drude mode (feature *α*) in the metallic state is lower compared to that of bulk-like metallic VO_2 [refs. [3,33]]. Importantly, we observe an optical interband transition (feature β′) in the near-infrared in the metallic state which is similar to that seen in the optical conductivity of the insulating state (see Fig. 4a). Based on the features α and β′ in the optical conductivity of the metallic state of the ultrathin VO_2 film, we propose the following scenario. The weak Drude feature arises from delocalized carriers which appear at the Fermi level as a quasiparticle peak (QP). The e_g^π conduction band stays above the Fermi level and is therefore empty. This leads to the interband transition β′ across the energy gap. This interband energy gap remains in parts of momentum space, which can be considered to be a pseudogap. In contrast, bulk VO_2 is metallic in the rutile structure because the Fermi level crosses partly filled a_{1g} and e_g^π bands.

We have considered the possibility that part of the ultrathin film undergoes the IMT to a bulk-like rutile metal leading to coexisting metallic and insulating phases at $T = 330$ K (above the IMT T_c). We performed near-field infrared microscopy experiments that are sensitive to in-plane and out-of-plane inhomogeneity[3,44]. Figure 5 shows scattering-type scanning near-field infrared microscopy (s-SNIM) images taken on the 7.2 nm VO_2 on (001) TiO_2. It is clear that, in the fully insulating phase ($T = 300$ K) and fully metallic phase ($T = 330$ K), the film displays uniform infrared properties and there is no phase coexistence. There is phase coexistence at the intermediate temperatures. Images were obtained using a Neaspec GmbH near-field microscope with an Arrow NCPt (Non-Contact Pt) tip illuminated by ~10 μm wavelength from a CO_2 laser. The near-field signal was obtained by operating the microscope in the pseudo-heterodyne detection scheme[45]. The signal was detected by an MCT detector and was demodulated at the third harmonic of the tip tapping frequency.

Further support for the empty e_g^π conduction bands in ultrathin rutile metallic VO_2 comes from the relatively small change in feature ξ between the insulating and metallic states (see Fig. 4a). Feature ξ consists of optical interband transitions from the filled O_{2p} band to the e_g^π band[33]. However, it is dominated by spectral weight of the interband transitions from the filled O_{2p} band to the e_g^π band as the optical selection rule favors optical transition when there is a change of unity in the orbital angular momentum of the electrons like that between *p*-orbitals and *d*-orbitals. In bulk-like VO_2, there is a drastic reduction in the spectral weight of feature ξ because the empty e_g^π band in the insulating phase becomes partly occupied in the metallic phase (Fig. 4b, c). Clearly, the relatively small change in feature ξ between the insulating and metallic states in the ultrathin VO_2 film suggests that the e_g^π band is empty in the metallic state and downshifts by about 0.1 eV. Moreover, the spectral weight of feature ξ is shifted to the QP states in the metallic phase.

DISCUSSION

We discuss this research based on rutile insulator showing the absence of $d_\parallel^*$ states in the VO_2 films of thickness less than the defined critical value of ≈7.5 nm. We note that previous observations of $d_\parallel^*$ state of V-V dimers, reported and analyzed in ref. [39], and more recently measured by XAS (X-ray absorption spectroscopy) and HAXPES were done for epitaxial films with larger than 7 nm thickness grown on $VO_2/TiO_2(001)$ and $VO_2/TiO_2(100)$ (refs. [31] and [46]) and $VO_2/Nb:TiO_2(001)$ (ref. [40]). Above all, we review XAS in which an electron is promoted from a core-level to an empty orbital, thus, probing the empty levels, and O K-edge XAS that has been used to probe empty $d_\parallel^*$ state, associated with the V-V dimers formation[39]. However, XAS, as well as HAXPES, are not direct measurements of crystallographic structure. We notice in the published literature that often there is lack of atomic structure characterization of ultrathin VO_2 films by relevant XRD and TEM techniques. We think that our corresponding results (Figs. 1b–d, 2b–d, 3b) fill the void. Moreover, we also performed indirect measurement of the V-V dimer associated interband peaks by broadband infrared and optical spectroscopy (Fig. 4), and obtained results consistent with those acquired by direct tools like XRD and TEM.

In ref. [31], the results of XAS and HAXPES for epitaxial 10 nm-thick (above ≈7.5 nm critical thickness) VO_2 ($T_c \approx 0$ °C or 278 K) on $TiO_2(001)$ showed $d_\parallel^*$ indicating the V-V dimer below T_c, which is consistent with our results. However, an epitaxial 5 nm-VO_2 ($T_c \approx 100$ °C or 378 K) on $TiO_2(100)$ also displayed the $d_\parallel^*$ band. On the basis of different T_c's, we can suggest that the epitaxial film

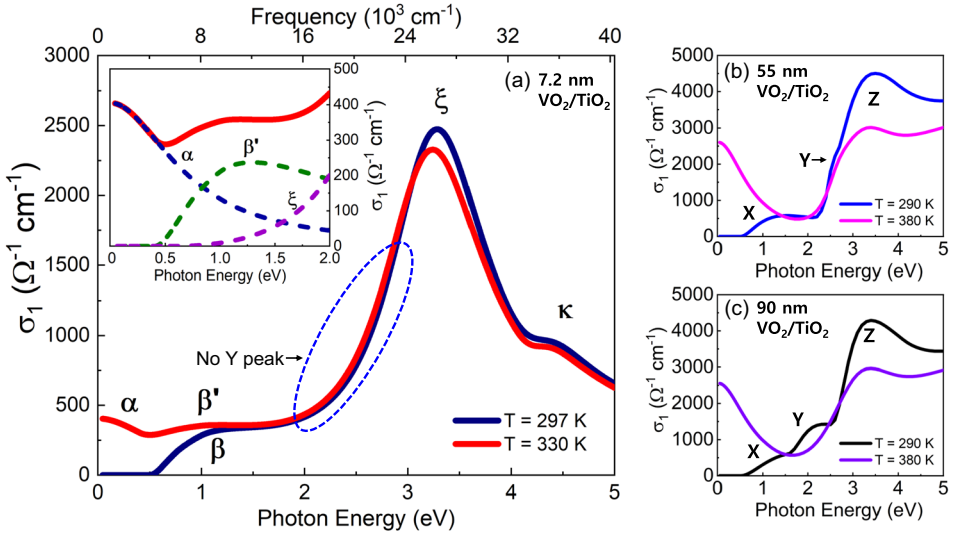

Fig. 4 Optical conductivity of VO_2 films. a Real part of the optical conductivity (σ_1) for the insulating (dark blue) and metallic (red) phases of the 7.2 nm thick VO_2 film on rutile (001) TiO_2 as a function of photon energy. (inset) Zoomed in low energy region of σ_1 in the metallic phase. The dashed lines representing individual contributions of the free carrier Drude feature, α (blue), and the optical transitions, β′ (green) and ξ (purple). **b** Plot of σ_1 in the insulating (blue) and metallic (magenta) phases of a thick 55 nm VO_2 film grown on rutile (001) TiO_2. **c** Plot of σ_1 in the insulating (black) and metallic (purple) phases of a thick 90 nm VO_2 film grown on rutile (001) TiO_2. As expected, the Y peak in the thicker 90 nm film is more prominent than in the 55 nm thick film. The Y peak is also slightly red-shifted in the 90 nm thick film due to a higher degree of strain relaxation compared to the 55 nm thick film.

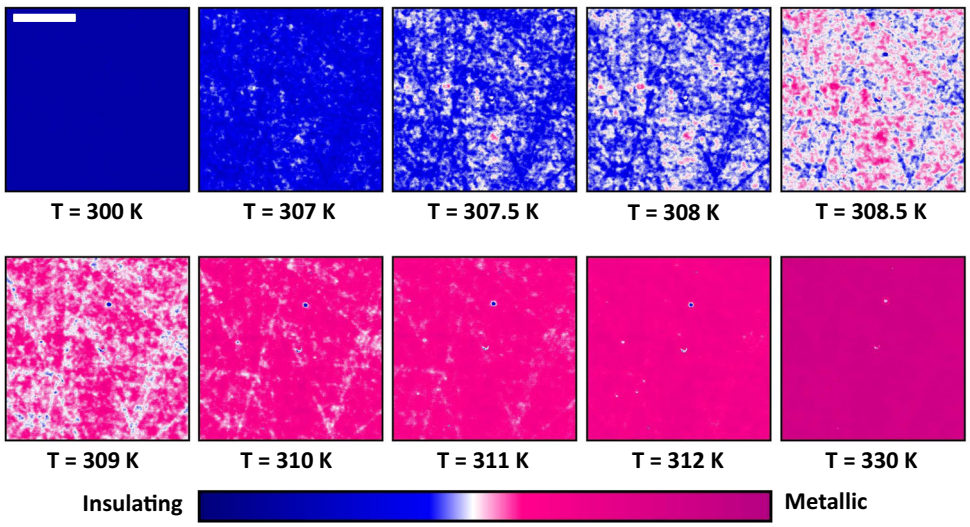

Fig. 5 S-SNIM images of a VO_2 film. S-SNIM images of the 7.2 nm VO_2 film on (001) TiO_2 obtained while heating through the transition. White scale bar represents 2 μm. The film is in the fully insulating phase (uniform dark blue color) at $T = 300$ K and fully metallic phase at $T = 330$ K (uniform dark pink color). There are coexisting insulating and metallic phases at intermediate temperatures.

on TiO_2(100) has completely different type and level of strain than the epitaxial film on TiO_2(001). Moreover, the VO_2/TiO_2(100) sample is beyond our research scope.

Subsequently, VO_2 films below 10 nm thickness on Nb-doped TiO_2(001) obtained d||* band by XAS experiments[40]. This is a discrepancy with the results of rutile insulator proposed by X-ray and optical measurements in this research, which may be caused by a difference in lattice constants of TiO_2 and Nb-doped TiO_2 substrates, resulting in different strain imposed on the films. Nb with a larger than Ti ionic radius, as a substitute of Ti in TiO_2 lattice, may cause distortions. Moreover, pure TiO_2 is a good insulator, whereas Nb-doped TiO_2 is conducting, and this difference in electrical conductivity of the substrates may affect properties of ultrathin films grown on these two different types of substrates. Also, the difference may be explained by different growth conditions of the films, which can be also confirmed by differences in resistance-temperature curves measured in our work and in ref. [40]. Nevertheless, these differences allowed us to stabilize the rutile insulating phase for up to 7.2 nm-VO_2 film, that is confirmed by direct and indirect measurements of VO_2 lattice and electronic structure.

Moreover, as for ref. [46], even though it shows an important scientific result, we note this work is related to VO_2 films with different strain effect grown on TiO_2 (100), while our work focuses on the VO_2 films on TiO_2 (001). These two types of samples are very different due to difference in the in-plane lattice constants of the substrates. Thus, in the case of TiO_2 (100), *b*-axis (~4.59 Å) and *c*-axis (~2.96 Å) are in-plane, while in the case of TiO_2 (001), *a*-axis

(~4.59 Å) and *b*-axis (~4.59 Å) are in-plane. The different lengths of the *a*- and c- lattice constants results in a very different tensile/compressive strain in the VO_2 films grown on TiO_2 (100) and TiO_2 (001), very different T_c values (77.6 °C vs 19.1 °C), and different transition pathway, as described in ref. [31].

We review first-principles DFT/DMFT research on the IMT in rutile VO_2 structure in the presence of strain. The DFT + U (Density Functional Theory with the Hubbard electron–electron correlation parameter *U*) calculations showed that in the ultrathin VO_2 locked by epitaxial strain in the rutile structure, the change in the electronic state from insulating to metallic can occur by means of changing the *U* value only from 4.5 to 0.0 eV[22]. Moreover, on the basis of cluster-DMFT (dynamic mean field theory) calculations, it was proposed that under the influence of small external strain, the rutile VO_2 phase can support either metallic or insulating states, or coexistence of both[38]. In particular, it was also shown that the insulating rutile phase can be stabilized in the case of large (about 3.5 eV) values of on-site Hubbard *U*[38]. We believe our experimental results will further stimulate first-principles theoretical studies.

The Ginzburg–Landau (G–L) calculations of strained VO_2 films in ref. [31] are interesting but provide limited information. The authors of ref. [31] clearly admit that the G-L calculations *qualitatively* track their experimental results. There are obvious quantitative discrepancies. For example, the experimental T_c of the insulator-metal transition (IMT) in VO_2 on (001) TiO_2 is about 20 °C lower than the temperature of the structural-phase transition (SPT) between monoclinic and rutile predicted by the G–L theory. The discrepancy between experiment and G–L theory comes from the different mechanisms of the IMT and the SPT. Moreover, it is well-known that G–L theory is a general, phenomenological theory. The G–L theory may provide a qualitative, macroscopic description of the SPT, but it does not provide insight into the microscopic IMT mechanism.

In conclusion, the rutile insulator and the absence of bonding-antibonding CDW gap are discovered in the ultrathin VO_2 films with thickness below 7.5 nm grown by PLD on rutile (001) TiO_2 substrates. This suggests a purely electronic IMT in the rutile structure of VO_2 without the SPT. This result is an important extension of the previously observed IMT without the SPT[4,47]. Moreover, it was suggested that in addition to electron–electron correlations, impurities play a decisive role in the IMT as well[47–50]. As the surface and interface has many kinds of impurities including oxygen vacancies induced by terraces, facets, and cracks, etc[10,34,35], and defects induced by shear stress coming from lattice mismatch between substrate and thin film, it follows that impurities may induce the IMT[47–50]. Moreover, as another evidence of the influence of impurities, it is well known that the resistance jump ratio of 2.5 orders-of-magnitude in VO_2/TiO_2 films at T_c, as shown in Figs. 1a, 2a, and 3a, is smaller than that of about 4 orders-of-magnitude in thick VO_2/Al_2O_3 films and a good VO_2 single crystal. This difference results from the exponential characteristic below T_c of extrinsic semiconductors (with impurities of 0.018%) that are not able to generate the SPT[47].

METHODS

Film growth conditions

The ultrathin VO_2 films were grown on rutile (001) TiO_2 substrates at 500 °C via pulsed laser deposition. A KrF excimer laser was used to ablate a metallic vanadium target with a pulse energy of 300 mJ and a repetition rate of 10 Hz. The oxygen pressure was maintained at 20 mTorr while growing and cooling of the sample.

X-ray diffraction measurements

To highlight the growth quality of VO_2, as well as evolution of its properties across the phase transition, both electrical and structural measurements were performed as a function of temperature. The electrical resistance of the films was acquired using a conventional four-probe system (JANIS CCS-450) equipped with a resistive heater to provide the sample heating up to 350 K. The temperature values were measured by two silicon diode thermometers integrated with an automatic temperature controller. The crystalline structure of the 7.2 nm thick VO_2 film was evaluated by variable temperature X-ray diffractometer (RIGAKU, D/MAX-2500) using Cu Kα radiation with an operating voltage of 40 kV and current of 300 mA. The sample was heated up with a rate 1 °C/min and stabilized for 3 min at a particular temperature prior to performing the continuous theta-2theta scans with a 0.01° step. Temperature dependent XRD measurements on the 7.2 nm thick VO_2 film on rutile (001) TiO_2 substrate are shown in Supplementary Fig. 2a. An obvious feature from the rutile (001) TiO_2 substrate is seen in the data. There is also a broad VO_2 feature centered at $2\theta \approx 66°$ that is independent of temperature indicating that the ultrathin VO_2 film maintains the rutile structure across the IMT.

TEM measurements

The ultrathin VO_2 film used for optical measurements is 7.2 nm thick as determined by grazing-angle X-ray reflectivity (XRR) measurement (see Supplementary Fig. 2b). Grazing-angle XRR measurements were obtained with a Panalytical Empyrean X-ray diffractometer. Atomic Force Microscopy (AFM) scans reveal the film's surface to be very smooth with an rms roughness of 0.2 nm. Epitaxial growth was confirmed by TEM (Fig. 1). For TEM experiments, thin samples that are transparent to electrons were prepared by a focused-ion beam technique using Ga ions as a polisher. The microstructural characterizations were done via cross-sectional observations of VO_2/TiO_2 with High-Resolution TEM operated at 300 kV. The obtained images were analyzed with DigitalMicrograph software (Gatan Inc.).

XRD measurements using a synchrotron light source

Synchrotron XRD measurements were conducted at the BXDS-WLE beamline in the Canadian Light Source. X-ray energy of 15.120 keV was selected by Si(111) monochromator. Samples were mounted on the heating-cooling stage of HFS350-GI (Linkam Scientific Instruments Inc.) by using a silver epoxy. A K-type thermocouple was attached on the sample stage also by using the silver epoxy. During a low temperature measurement a dry nitrogen gas was blown over the sample to prevent condensation of water moisture. Mythen2 1K, a one dimensional detector from Dectris, was mounted on a detector arm and placed at desired two-theta angles. The sample-to-detector distance was 1128 mm.

Optical measurements and analysis

Spectroscopic ellipsometry at 70° and 75° angles of incidence was performed on the 7.2 nm thick VO_2 film on rutile (001) TiO_2 substrate and on the pristine rutile (001) TiO_2 substrate for photon energies 0.6–6.5 eV (4800 to 52,000 cm^{-1}) using the Variable-Angle Spectroscopic Ellipsometer (VASE) from J. A. Woollam Co., Inc. The ellipsometry data was complemented by mid- and far-infrared spectroscopy measurements performed in normal incidence transmission and near-normal incidence reflectance geometries from photon energies 50–740 meV (400–6000 cm^{-1}) in a Bruker Vertex 80v Fourier Transform Infrared (FTIR) spectrometer. For all spectroscopy measurements, the sample temperature was varied and monitored using a Lakeshore temperature controller, resistive heaters, silicon diode thermometer, and home-built heating stages to take data above and below T_c.

Kramers-Kronig consistent oscillators were employed in the substrate model to fit the ellipsometry, transmission, and reflectance data on the pristine TiO_2 substrate using W-VASE software from J. A. Woollam Co., Inc. Next, the ellipsometry, transmission and reflectance data from the VO_2 films on the substrate was modeled by adding a VO_2 layer to the TiO_2 substrate model. The thickness of the VO_2 layer was equal to the VO_2 film thickness. The data was fit using Kramers–Kronig consistent oscillators in the VO_2 layer. Thus, we obtain the broadband dielectric function of the VO_2 film above and below the IMT temperature (see Supplementary Fig. 3). The real and imaginary parts of the dielectric function are used respectively to obtain the imaginary and real parts of the optical conductivity. Due to the ultrathin nature of the film, we do not observe VO_2 phonon features in the mid- and far-infrared reflectance spectrum which is dominated by the phonons of the TiO_2 substrate.

The effective number of delocalized carriers per vanadium atom, N_{eff}^{Drude}, in the metallic state can be calculated from the conductivity $\sigma_1^{Drude}(\omega)$ of the Drude oscillator used in the fits to the infrared and optical

spectroscopy data (Fig. 4a, inset).

$$N_{\mathrm{eff}}^{\mathrm{Drude}} = \frac{m_0 V_0 \omega_{\mathrm{p}}^2}{4\pi e^2} = \frac{2m_0 V_0}{\pi e^2}\int_0^{\infty} \sigma_1^{\mathrm{Drude}}(\omega)\mathrm{d}\omega \quad (1)$$

Here, V_0 is the cell volume of one VO_2 formula unit in the rutile structure and ω_p is the Drude plasma frequency[37]. The delocalized carriers are assumed to have free-electron mass (m_0). We find that the plasma frequency $\omega_p = 1.32$ eV, and ω_p^2 is about four times lower than the value for bulk-like rutile VO_2 metal. We find that $N_{\mathrm{eff}}^{\mathrm{Drude}}$ is about 0.037 and our calculations of $N_{\mathrm{eff}}^{\mathrm{Drude}}$ in the ultrathin VO_2 film are a lower bound, because it is likely the mass of the delocalized carriers is larger than the free electron mass assumed in the $N_{\mathrm{eff}}^{\mathrm{Drude}}$ calculations. Using the relaxation time (τ) of the Drude oscillator, we obtain a scattering rate $1/(2\pi c\tau) = 5.6 \times 10^3\ \mathrm{cm}^{-1}$, where c is the speed of light. The scattering rate is notably higher than that seen in bulk-like VO_2 film and this suggests stronger electronic correlations[51].

DATA AVAILABILITY

The datasets generated during and/or analyzed during the current study are available from the corresponding authors on reasonable request.

Received: 15 February 2021; Accepted: 14 June 2022;
Published online: 12 July 2022

REFERENCES

1. Dobrosavljevic, V., Trivedi, N. & Valles, J. M. *Conductor-Insulator Quantum Phase Transitions* 3–58 (Oxford University Press, 2012).
2. Rice, T. M., Launois, H. & Pouget, J. Comment on "VO_2': Peierls or Mott–Hubbard? a view from band theory". *Phys. Rev. Lett.* **73**, 3042 (1994).
3. Qazilbash, M. M. et al. Mott transition in VO_2 revealed by infrared spectroscopy and nano-imaging. *Science* **318**, 1750–1753 (2007).
4. Kim, H. T. et al. Monoclinic and correlated metal phase in VO_2 as evidence of the Mott transition: Coherent phonon analysis. *Phys. Rev. Lett.* **97**, 266401 (2006).
5. Goodenough, J. B. The two components of the crystallographic transition in VO_2. *J. Solid State Chem.* **3**, 490–500 (1971).
6. Wentzcovitch, R. M., Schulz, W. W. & Allen, P. B. VO_2: Peierls or Mott–Hubbard? A view from band theory. *Phys. Rev. Lett.* **72**, 3389–3392 (1994).
7. Matsuda, Y. H. et al. Magnetic-field-induced insulator–metal transition in W-doped VO_2 at 500 T. *Nat. Commun.* **11**, 3591 (2020).
8. Zhang, Y., Xiong, W., Chen, W. & Zheng, Y. Recent progress on vanadium dioxide nanostructures and devices: Fabrication, properties, applications, and perspectives. *Nanomaterials* **11**, 338 (2021).
9. Nájera, O., Civelli, M., Dobrosavljević, V. & Rozenberg, M. J. Resolving the VO_2 controversy: Mott mechanism dominates the insulator-to-metal transition. *Phys. Rev. B* **95**, 035113 (2017).
10. Weber, C. et al. Vanadium dioxide: A Peierls–Mott insulator stable against disorder. *Phys. Rev. Lett.* **108**, 256402 (2012).
11. Brito, W. H., Aguiar, M. C. O., Haule, K. & Kotliar, G. Metal–insulator transition in VO_2: A DFT + DMFT perspective. *Phys. Rev. Lett.* **117**, 056402 (2016).
12. Okazaki, K., Sugai, S., Muraoka, Y. & Hiroi, Z. Role of electron–electron and electron–phonon interaction effects in the optical conductivity of VO_2. *Phys. Rev. B* **73**, 165116 (2006).
13. Kawatani, K., Kanki, T. & Tanaka, H. Formation mechanism of a microscale domain and effect on transport properties in strained VO_2 thin films on TiO_2 (001). *Phys. Rev. B* **90**, 054203 (2014).
14. Sohn, A., Kanki, T., Tanaka, H. & Kim, D. W. Visualization of local phase transition behaviors near dislocations in epitaxial VO_2/TiO_2 thin films. *Appl. Phys. Lett.* **107**, 171603 (2015).
15. Shiga, D. et al. Emergence of metallic monoclinic states of VO_2 films induced by K deposition. *Phys. Rev. B* **99**, 125120 (2019).
16. Sharma, Y. et al. Competing phases in epitaxial vanadium dioxide at nanoscale. *Appl. Phys. Lett. Mater.* **7**, 081127 (2019).
17. Eguchi, R. et al. Photoemission evidence for a Mott–Hubbard metal-insulator transition in VO_2. *Phys. Rev. B* **78**, 075115 (2008).
18. Kittiwatanakul, S., Wolf, S. A. & Lu, J. Large epitaxial bi-axial strain induces a Mott-like phase transition in VO_2. *Appl. Phys. Lett.* **105**, 073112 (2014).
19. Paik, H. et al. Transport properties of ultra-thin VO_2 films on (001) TiO_2 grown by reactive molecular-beam epitaxy. *Appl. Phys. Lett.* **107**, 163101 (2015).
20. Paez, G. J. et al. Simultaneous structural and electronic transitions in epitaxial VO_2/TiO_2 (001). *Phys. Rev. Lett.* **124**, 196402 (2020).
21. Qiu, H. et al. The tetragonal-like to rutile structural phase transition in epitaxial VO_2/TiO_2 (001) thick films. *N. J. Phys.* **17**, 113016 (2015).
22. Yang, M. et al. Suppression of structural phase transition in VO_2 by epitaxial strain in vicinity of metal–insulator transition. *Sci. Rep.* **6**, 23119 (2016).
23. Creeden, J. A. et al. Structural and photoelectric properties of epitaxially grown vanadium dioxide thin films on *c*-plane sapphire and titanium dioxide. *Sci. Rep.* **9**, 9362 (2019).
24. Suess, R. J. et al. Ultrafast phase transition dynamics in strained vanadium dioxide films. *Adv. Mater. Interfaces* **4**, 1700810 (2017).
25. Cho, Y. et al. Morphology of phase-separated VO_2 films deposited on TiO_2-(001) substrate. *Mater. Res. Bull.* **102**, 289–293 (2018).
26. Gray, A. X. et al. Correlation-driven insulator–metal transition in near-ideal vanadium dioxide films. *Phys. Rev. Lett.* **116**, 116403 (2016).
27. D'Elia, A. et al. Detection of spin polarized band in VO_2/TiO_2 (001) strained films via orbital selective constant initial state spectroscopy. *Condens. Matter* **5**, 72 (2020).
28. Quackenbush, N. F. et al. Nature of the metal insulator transition in ultrathin epitaxial vanadium dioxide. *Nano Lett.* **13**, 4857–4861 (2013).
29. Fan, L. L. et al. Strain dynamics of ultrathin VO_2 film grown on TiO_2 (001) and the associated phase transition modulation. *Nano Lett.* **14**, 4036–4043 (2014).
30. Evlyukhin, E. et al. Directly measuring the structural transition pathways of strain-engineered VO_2 thin films. *Nanoscale* **12**, 18857–18863 (2020).
31. Quackenbush, N. F. et al. Stability of the M2 phase of vanadium dioxide induced by coherent epitaxial strain. *Phys. Rev. B* **94**, 085105 (2016).
32. Haverkort, M. W. et al. Orbital-assisted metal–insulator transition in VO_2. *Phys. Rev. Lett.* **95**, 196404 (2005).
33. Qazilbash, M. M. et al. Electrodynamics of the vanadium oxides VO_2 and V_2O_3. *Phys. Rev. B* **77**, 115121 (2008).
34. Wahila, M. J. et al. The breakdown of Mott physics at VO_2 surfaces. Preprint at https://arxiv.org/abs/2012.05306 (2020).
35. Krisponeit, J.-O. et al. The morphology of VO_2/TiO_2(001): Terraces, facets, and cracks. *Sci. Rep.* **10**, 22374 (2020).
36. Lebrun, J. M. et al. Broadening of diffraction peak widths and temperature nonuniformity during flash experiments. *J. Am. Ceram. Soc.* **99**, 3429–3434 (2016).
37. Dressel, M. & Gruner, G. *Electrodynamics of Solids* (Cambridge University Press, 2002).
38. Lazarovits, B., Kim, K., Haule, K. & Kotliar, G. Effects of strain on the electronic structure of VO_2. *Phys. Rev. B* **81**, 115117 (2010).
39. Koethe, T. C. et al. Transfer of spectral weight and symmetry across the metal–insulator transition in VO_2. *Phys. Rev. Lett.* **97**, 116402 (2006).
40. Shiga, D. et al. Thickness dependence of electronic structures in VO_2 ultrathin films: Suppression of the cooperative Mott–Peierls transition. *Phys. Rev. B* **102**, 115114 (2020).
41. Verleur, H. W., Barker, A. S. & Berglund, C. N. Optical properties of VO_2 between 0.25 and 5 eV. *Phys. Rev.* **172**, 788–798 (1968).
42. Huffman, T. J. et al. Modification of electronic structure in compressively strained vanadium dioxide films. *Phys. Rev. B* **91**, 205140 (2015).
43. Sun, J. & Pribil, G. K. Analyzing optical properties of thin vanadium oxide films through semiconductor-to-metal phase transition using spectroscopic ellipsometry. *Appl. Surf. Sci.* **421**, 819–823 (2017).
44. Krutokhvostov, R. et al. Enhanced resolution in subsurface near-field optical microscopy. *Opt. Express* **20**, 593–600 (2012).
45. Ocelic, N., Huber, A. & Hillenbrand, R. Pseudoheterodyne detection for background-free near-field spectroscopy. *Appl. Phys. Lett.* **89**, 101124 (2006).
46. Quackenbush, N. F. et al. X-ray spectroscopy of ultra-thin oxide/oxide heteroepitaxial films: A case study of single-nanometer VO_2/TiO_2. *Materials* **8**, 5452–5466 (2015).
47. Kim, H. T. et al. Mechanism and observation of Mott transition in VO_2-based two- and three-terminal devices. *N. J. Phys.* **6**, 52 (2004).
48. Kim, H. T. Impurity-driven insulator-to-metal transition in VO_2. *Jpn. Phys. Soc.* **71.2**, 13aJB–1 (2016).
49. Kim, H. T. et al. Photoheat-induced Schottky nanojunction and indirect Mott transition in VO_2: Photocurrent analysis. *J. Phys. Condens. Matter* **28**, 085602 (2016).
50. Kim, C.-Y., Slusar, T., Cho, J. & Kim, H.-T. Mott switching and structural transition in the metal phase of VO_2 nanodomain. *ACS Appl. Electron. Mater.* **3**, 605–610 (2021).
51. Qazilbash, M. M. et al. Correlated metallic state of vanadium dioxide. *Phys. Rev. B* **74**, 205118 (2006).

ACKNOWLEDGEMENTS

This work was supported by Institute of Information & Communications Technology Planning & Evaluation (IITP) grant funded by the Korean government (MSIT) via Grant 2017-0-00830. Part of the research described in this paper was performed at the Canadian Light Source, a national research facility of the University of Saskatchewan, which is supported by the Canada Foundation for Innovation (CFI), the Natural Sciences and Engineering Research Council (NSERC), the National Research Council

(NRC), the Canadian Institutes of Health Research (CIHR), the Government of Saskatchewan, and the University of Saskatchewan.

AUTHOR CONTRIBUTIONS

The William & Mary group and ETRI group contributed equally to this work. D.J.L. is the first coauthor from W&M group, and T.S. is the first coauthor from ETRI group. M.M.Q. and H.T.K. conceived the project. M.M.Q. and H.T.K. wrote the manuscript with contributions from all other coauthors. D.J.L., T.S., D.B.B., and C.Y.K. performed the experiments and data analysis. H.J. contributed to the optical data analysis.

COMPETING INTERESTS

The authors declare no competing interests.

ADDITIONAL INFORMATION

Supplementary information The online version contains supplementary material available at https://doi.org/10.1038/s41535-022-00479-x.

Correspondence and requests for materials should be addressed to Hyun-Tak Kim or M. M. Qazilbash.